Dyes and Pigments 82 (2009) 76–83

Contents lists available at ScienceDirect

Dyes and Pigments

journal homepage: www.elsevier.com/locate/dyepig

Nonlinear optical, poly(amide-imide)–clay nanocomposites comprising an azobenzene moiety synthesised via sequential self-repetitive reaction

Hsun-Lien Lin [a], Huey-Ling Chang [b,**], Tzong-Yuan Juang [c], Rong-Ho Lee [d], Shenghong A. Dai [a], Ying-Ling Liu [e], Ru-Jong Jeng [a,*]

[a] Department of Chemical Engineering, National Chung Hsing University, 250 Kuo-Kuang Road, Taichung 402, Taiwan
[b] Department of Chemical and Materials Engineering, National Chinyi University of Technology, Taichung 411, Taiwan
[c] Department of Applied Chemistry, National Chiayi University, Chiayi 60004, Taiwan
[d] Department of Chemical Engineering, National Yunlin University of Science and Technology, Yunlin 640, Taiwan
[e] Department of Chemical Engineering and R&D Center for Membrane Technology, Chung Yuan Christian University, Taoyuan 320, Taiwan

ARTICLE INFO

Article history:
Received 19 July 2008
Received in revised form
18 November 2008
Accepted 18 November 2008
Available online 3 December 2008

Keywords:
Azobenzene
Montmorillonite
Sequential self-repetitive reaction
Nonlinear optical properties
Poly(amide-imide)
Nanocomposite

ABSTRACT

Poly(*N*-acylurea)–clay nanocomposites consisting of a modified montmorillonite and poly(*N*-acylurea) were prepared from which poly(amide-imide)–clay nanocomposites were subsequently obtained via the sequential self-repetitive reaction of poly(*N*-acylurea). The moderate T_g of poly(*N*-acylurea) allows the nonlinear optically active polymer to exhibit high poling efficiency; in situ poling and curing increased the T_gs of poly(amide-imide)–clay nanocomposites. Electro-optical coefficients, r_{33} of ~17–20 pm/V (830 nm), were achieved; high temporal stability (120 °C) and waveguide optical losses of 3.4–3.9 dB/cm at 1310 nm were also obtained for poly(amide-imide)–clay nanocomposites.

© 2008 Elsevier Ltd. All rights reserved.

1. Introduction

Second-order nonlinear optical (NLO) polymers have been of great interest for many years due to their potential applications in photonic devices [1–6]. The key requirements imposed on the NLO polymers include large optical nonlinearities and excellent temporal stability at 80–125 °C [7–15]. To enhance the stability, one approach is to introduce the inorganic component into the organic NLO materials, yielding organic/inorganic hybrid materials via a sol–gel process [16–18]. In our recent investigation [19], NLO-active poly(amide-imide)s obtained via sequential self-repetitive reaction (SSRR) have been systematically studied. In addition, organic/inorganic NLO-active nanocomposites were prepared by performing SSRR of poly(*N*-acylurea) and sol–gel process of phenyltriethoxysilane, concurrently [20]. Because of the formation of the three-dimensional silicon oxide networks, long-term NLO stability at elevated temperatures was greatly enhanced. However, this enhancement usually requires the presence of large quantities of the inorganic sol–gel materials in polymer matrices. This would lead to a reduced loading of dye content, meaning the decrease of optical nonlinearity.

A system based on two-dimensional smectite clays distributed in the polymer matrices might provide another route for the polymeric materials with stable NLO response [21]. Smectite clay minerals, such as montmorillonite (MMT), having appropriate functional molecules in between the silicate layers (which is called intercalation) are supposed to exhibit a wide range of novel characteristics such as ion conductivity and unusual electric and NLO properties [22–26]. In our previous investigation [25], the polyimide/MMT materials show much better long-term NLO stability at elevated temperatures than the pristine polyimide. By dispersing a small amount of nano-scaled organoclay into the poly(amic acid), both the imidization temperature and the time of poly(amic acid) can also be reduced dramatically [27,28]. A lower imidization temperature would help in enhancing the poling efficiency, i.e. NLO properties [20].

In this research, we report a series of new NLO-active poly(amide-imide)–clay materials prepared via SSRR [19,29]. Difunctional diamino diphenyl methane (DDM) was chosen to be the intercalating agent. One of the functional groups would form

* Corresponding author. Tel.: +886 4 22852581; fax: +886 4 22854734.
** Corresponding author.
E-mail address: rjjeng@nchu.edu.tw (R.-J. Jeng).

0143-7208/$ – see front matter © 2008 Elsevier Ltd. All rights reserved.
doi:10.1016/j.dyepig.2008.11.005

an ionic bond with negatively charged silicates, whereas the remaining functional group of the intercalating agent is available for further reaction with anhydride groups of poly(*N*-acylurea). Because of the superb organo-solubility of poly(*N*-acylurea), the modified clay and poly(*N*-acylurea) could be easily processed into poly(*N*-acylurea)–clay nanocomposites for further SSRR process. In addition, a large number of anhydride groups are located throughout the poly(*N*-acylurea) chains, which are available for reactions with the amino groups of modified clay, resulting in greater interaction force to achieve excellent dispersion of layered silicates in the polymeric matrices. Poly(-amide-imide)–clay nanocomposites were obtained by performing SSRR of poly(*N*-acylurea)–clay during the in situ curing/poling processes at elevated temperatures. As the reaction temperature was raised up to 150 °C, poly(*N*-acylurea) would selectively decompose to form isocyanate, amide, and the isocyanate moieties, and then reacts with the carboxylic acid from anhydride to form thermally stable amide–imide linkage via the mechanism of SSRR. The moderate glass transition temperature (T_g) characteristic of poly(*N*-acylurea)–clay allows the NLO-active polymer to exhibit high poling efficiency. These poly(amide-imide)–clay nanocomposites would exhibit much better long-term NLO stability as compared to the pristine poly(amide-imide) sample.

2. Experimental

2.1. Preparation of NLO-active poly(amide-imide)–clay nanocomposites

All chemicals were used as received unless otherwise stated. The solvents were purified by distillation under reduced pressure over calcium hydride. Na^+-MMT, supplied by Nanocor Co., America, is a sodium type cationic exchange resin of cationic exchange capacity (CEC) of 1.20 equiv kg^{-1}.

2.1.1. Preparation of poly(N-acylurea)–DNDA (PaDN) and poly(amide-imide)–DNDA (PIDN)

The synthesis of 2,4-diamino-4′-(4-nitrophenyl-diazenyl) azobenzene (DNDA) was performed according to our previous study [19]. DNDA (1 mmol) was dissolved in anhydrous *N*,*N*-dimethylformamide (DMF, 5 cm^3) at room temperature, which was followed by the immediate addition of 4,4′-methylene diphenylisocyanate (MDI, 6 mmol). The solution was stirred at 60 °C for 2 h. After the addition of 1,3-dimethyl-3-phospholene oxide (DMPO), poly-carbodiimide (poly-CDI) was obtained to which was added trimellitic anhydride (TMA, 5 mmol). The ensuing solution was maintained at 60 °C for another 6 h after which, the mixture was poured into anhydrous ethyl acetate (EA) to give a dark red solid which was collected by filtration, washed thoroughly with EA and dried under vacuum at 80 °C. The number average molecular weight (M_n) and polydispersity index of PaDN were 54 200 and 3.08, respectively.

To obtain the DNDA-containing poly(amide-imide), poly(*N*-acylurea) was treated at 200 °C for 2 h; SSRR was achieved during this period of thermal treatment [19].

2.1.2. Preparation of MMT intercalated with DDM (MMT–DDM)

Na^+-MMT (1 g, 1.20 equiv kg^{-1}) was placed in a 250 cm^3 flask and dispersed vigorously in 100 cm^3 of deionized water at room temperature. In a separate vessel, the intercalating agent DDM (0.238 g, 1.20 mmol) was acidified with hydrochloric acid (37% in water, 0.18 g, 1.20 mmol, acidification molar ratio of H^+:NH_2 = 1:2) in 75 cm^3 of ethanol. The acidified DDM solution was poured into the flask containing the Na^+-MMT slurry and the ensuing mixture was stirred vigorously at 60 °C for 11 h and then allowed to cool to room temperature. The resulting agglomerated precipitate was collected and washed thoroughly with deionized water to remove free amine. The MMT–DDM obtained was dried in a vacuum oven at 70 °C and characterized using X-ray diffraction (XRD) and thermogravimetry analyses (TGA).

2.1.3. Synthesis of poly(N-acylurea)/MMT nanocomposite (PaM)

The synthesis of poly(*N*-acylurea)–clay nanocomposite (PaM) is shown in Fig. 1. PaDN was mixed with MMT–DDM in various mass ratios and the ensuing mixtures were stirred in DMF at room temperature for 6.5 h. PaM0.5, PaM1, PaM1.5, PaM2 and PaM3 of inorganic ratios of 0.5, 1.0, 1.5, 2.0 and 3.0, respectively, were prepared by drying.

2.1.4. Preparation of poly(amide-imide)/MMT nanocomposite (PIM)

To obtain poly(amide-imide)–clay nanocomposite (PIM), poly(*N*-acylurea)–clay, PaM was treated at 200 °C for 2 h (Fig. 1); SSRR was achieved during this period [19]. As a result, poly(amide-imide)–clay nanocomposites, PIM0.5, PIM1, PIM1.5, PIM2 and PIM3, were obtained with inorganic ratios of 0.5, 1.0, 1.5, 2.0 and 3.0, respectively.

2.2. Characterization of NLO-active polymers

Infrared spectra were recorded by using a Perkin Elmer Paragon 500 FT-IR spectrophotometer. ^{1}H NMR spectra were obtained with a Varian Gemini-300 FT-NMR spectrometer with DMSO-d_6. Elemental analysis was performed on an F002 Heraeus CHN–O rapid elemental analyzer employing acetanilide as a standard. DSC and TGA were performed on a Seiko SII Model SSC/5200. A heating rate of 10 °C/min under nitrogen atmosphere was used for DSC and TGA measurements. Thermal degradation temperature (T_d) is taken at 5% weight loss. A gel permeation chromatograph (Analytical Scientific Instruments Model 500) with a reflection index (RI) detector (Schambeck RI 2000) was used to measure the molecular weight relative to polystyrene standards. The carrier solvent was DMF at a flow rate of 1 ml/min. XRD analysis was performed with Shimadzu SD-Dl using a Cu target at 35 kV, 30 mA. The *d*-spacing of MMT was analyzed by using Bragg's equation ($n\lambda = 2d\sin\theta$). The morphology of the polymer was also analyzed by transmission electron microscopy (TEM, Zeiss EM 902A). TEM was operated at 80 kV and the sample widths of approximately 70 nm were microtomed at room temperature.

2.3. Thin film preparation and electro-optical (EO) coefficient measurements

2.3.1. Thin film preparation

Poly(*N*-acylurea)–clay nanocomposites and PaMs were each dissolved in DMF and the ensuing solution was filtered through a 1 μm filter. Thin films were prepared by spin-coating the filtered polymer solution onto indium tin oxide (ITO) glass substrates. Prior to the poling process, these thin films were dried in vacuum at 60 °C for 24 h.

The ellipsometric technique has been widely used for measuring the thin film thickness and other related characteristics [30]. This technique was used to measure the refractive indices using a variable angle spectroscopic ellipsometer (VASE), Model 2000D, from J.A. Woollam Co., Inc. The measurement temperature was maintained at 25 °C.

2.3.2. Poling process, EO coefficient (r_{33}) and optical loss measurement

EO coefficients of the poled samples were measured at 830 nm using the simple reflection technique [31]. The poling process for the second-order NLO polymer films was carried out using an in situ contact poling technique. The poling voltage was maintained at

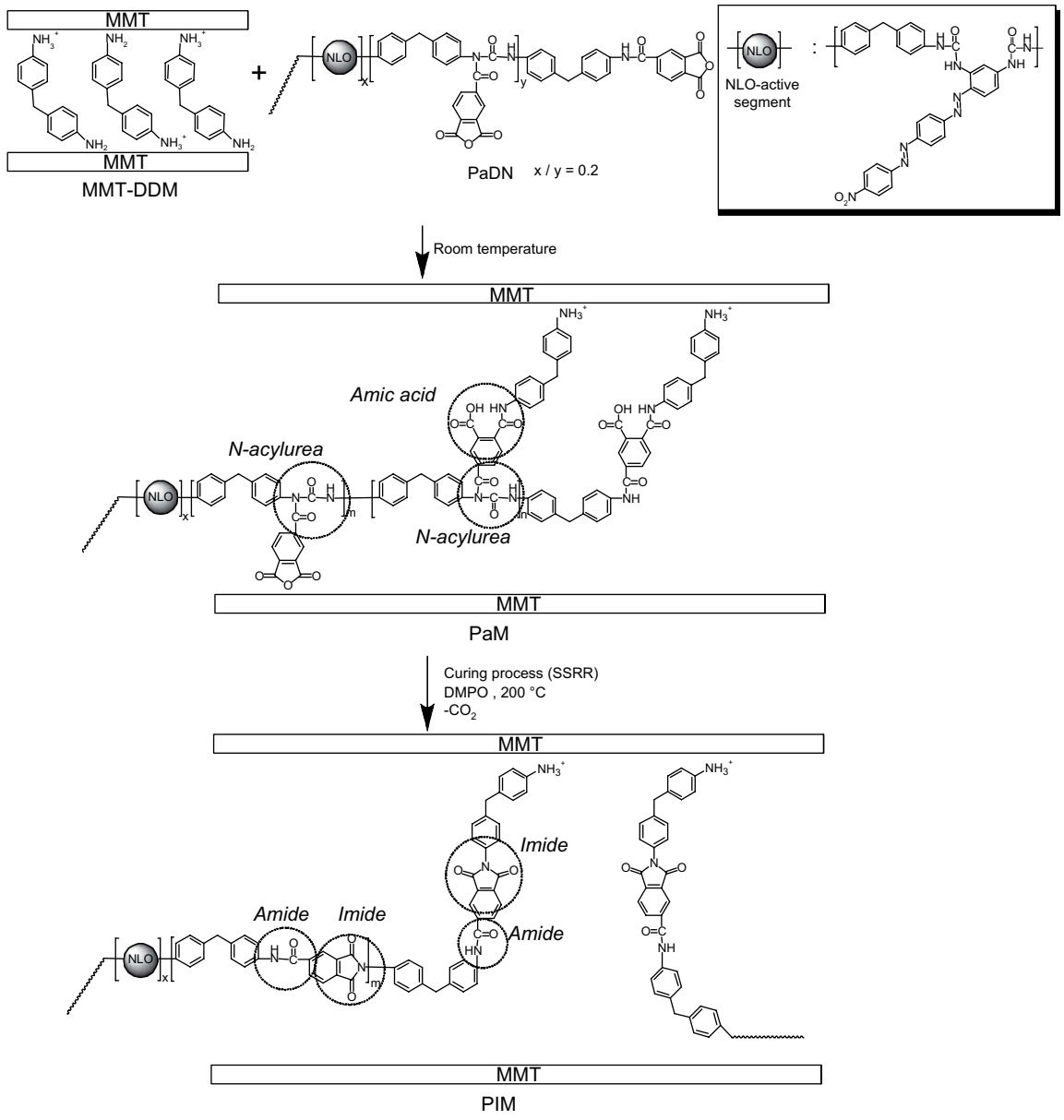

Fig. 1. Synthesis of PaM and PIM.

100 V and the temperature was kept at 200 °C for 2 h. The formation of the amide–imide linkages via SSRR and the alignment of dyes proceeded simultaneously during this period. The sample was then cooled down to room temperature in the presence of the poling field at which point the poling field was terminated. Optical losses of the polymer waveguides for poly(amide-imide)–clay nanocomposites were measured according to the literature [32]. The laser beam (830 and 1310 nm) first passes through a linear polarizer and a polarizing beam splitter, thus removing noise caused by polarizing fluctuations in the laser output. Rotation of the linear polarizer allows the intensity of the beam to be adjusted while rotation of the beam splitter allows for selection of TE polarized light. The un-reflected beam is focused onto a prism coupler that is mounted on a rotation stage. The scattered light is imaged with an infrared-sensitive charge-injection-device camera system. A distance scale is provided by imaging a ruler to provide a scale in pixels per centimeter. A statistical linear fit of the data to the logarithm of the scattered light intensity versus the distance propagated down the waveguide would yield a waveguide loss as a slope.

3. Results and discussion

3.1. Structural characterization of PaM and PIM

FT-IR spectroscopy was utilized to monitor the SSRR process of PaM nanocomposites. FT-IR spectra of PaM1.5 and its cured sample PIM1.5 are shown in Fig. 2. PaM1.5 was transformed into PIM1.5 via SSRR process. The sharp absorption peaks at around 1780 cm^{-1}, 1720 cm^{-1}, 1380 cm^{-1}, 1100 cm^{-1} and 726 cm^{-1} were identified as the formation of imide linkages for the cured sample. Those peaks at around 1646 cm^{-1} and 3300–3500 cm^{-1} were identified as the presence of amide groups. The completion of SSRR process was also indicated by the disappearance of anhydride absorption peak at around 1878 cm^{-1}. The FT-IR results demonstrate that the SSRR process proceeded successfully to form the PIM nanocomposite during the optimized curing/poling process. Before the SSRR process, a small number of the reactive functional groups, anhydrides, could react with the amino groups of the intercalating agent, DDM, forming amic acid. As the temperature rose to 200 °C,

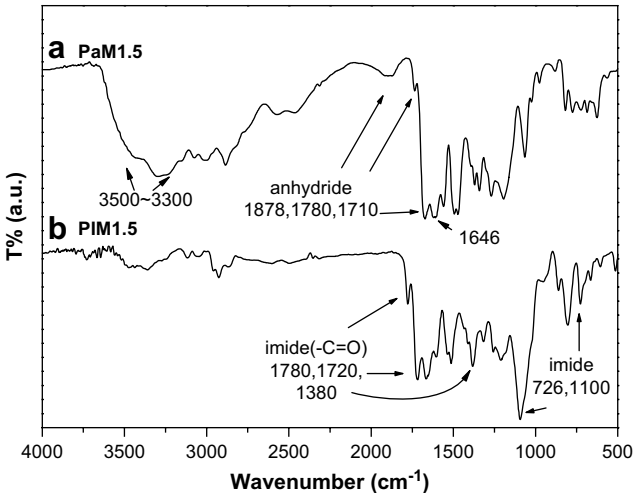

Fig. 2. Infrared spectra of (a) PaM1.5 and (b) cured PaM1.5, i.e. PIM1.5.

the isocyanates that decomposed from *N*-acylurea groups could either react with the nearby amino groups to form urea linkages, or react with anhydride groups to form imide linkages via SSRR as shown in Fig. 1. Therefore, several chemical-resistant linkages including urea, amide, and imide were present for the cured sample.

^{1}H NMR spectra of PaM1.5 and PIM1.5 in DMSO-d_6 are shown in Fig. 3. In ^{1}H NMR spectrum of PaM, a single peak for the proton of *N*-acylurea was observed at 10.4 ppm, indicating that poly(*N*-acylurea) was successfully synthesized. However, the proton of amic acid which was derived from the reaction between anhydride and amino group did not appear at around 10.0–10.3 ppm [33]. This is because only a small portion of anhydride functional groups would react with the 1.5 wt% amino containing organically modified MMT. In ^{1}H NMR spectrum of PIM, the peak at 10.4 ppm vanished and a new peak at 10.5 ppm emerged. This single peak at 10.5 ppm was the characteristic absorption of amide proton, indicating the completion of SSRR [29].

3.2. Morphology, solubility, and thermal stability of MMT–DDM and PIM

The intercalation of DDM into the Na^+-MMT interlayers was achieved by the exchange of sodium cations with stoichiometric amounts of DDM. The intercalation was confirmed via XRD and TGA analyses. XRD patterns of MMT and organically modified MMT–DDM are shown in Fig. 4. For the pristine MMT sample, the strong XRD peak at $2\theta = 7.4^\circ$ was caused by the diffraction of the (001) crystal surface of layered silicates. The *d*-spacing of MMT calculation based on Bragg's law ($n\lambda = 2d \sin\theta$, $2\theta = 7.4^\circ$) was 12 Å. For the MMT–DDM, the XRD peak was observed at $2\theta = 5.87^\circ$, equaling a *d*-spacing of 15 Å. Moreover, the organic/inorganic ratio of MMT–DDM (80.3 wt% char yield at 900 °C) was measured by TGA, conforming to the result calculated by CEC (19.7 wt% of DDM). The ionic groups of the silicate layers are almost completely saturated (97% of exchange). The lower concentration of Na^+ ions in the MMT indicates even lower concentration in the polymer matrices. Consequently, the presence of Na^+ ions would not pose a problem in electric poling. Hence, it is evident that DDM could effortlessly enlarge the spaces of MMT interlayers. As a result of that, MMT–DDM could be well-dispersed in DMF, toluene, THF and most of other organic solvents, leading MMT–DDM to be compatible with organic polymer matrices.

XRD patterns of poly(amide-imide)–clay nanocomposites, PIM0.5–PIM3, are shown in Fig. 4. The WAXD patterns of all the series of PIM samples containing 0.5–3 wt% inorganic content did not display any diffraction peak at $2\theta = 2$–10°, indicating that the *d*-spacings of silicate layers were intercalated to a distance of more than 59 Å or an exfoliated morphology was obtained. This is because the anhydride functional groups of PaDN could react with the amino groups of intercalating agents. Consequently, the

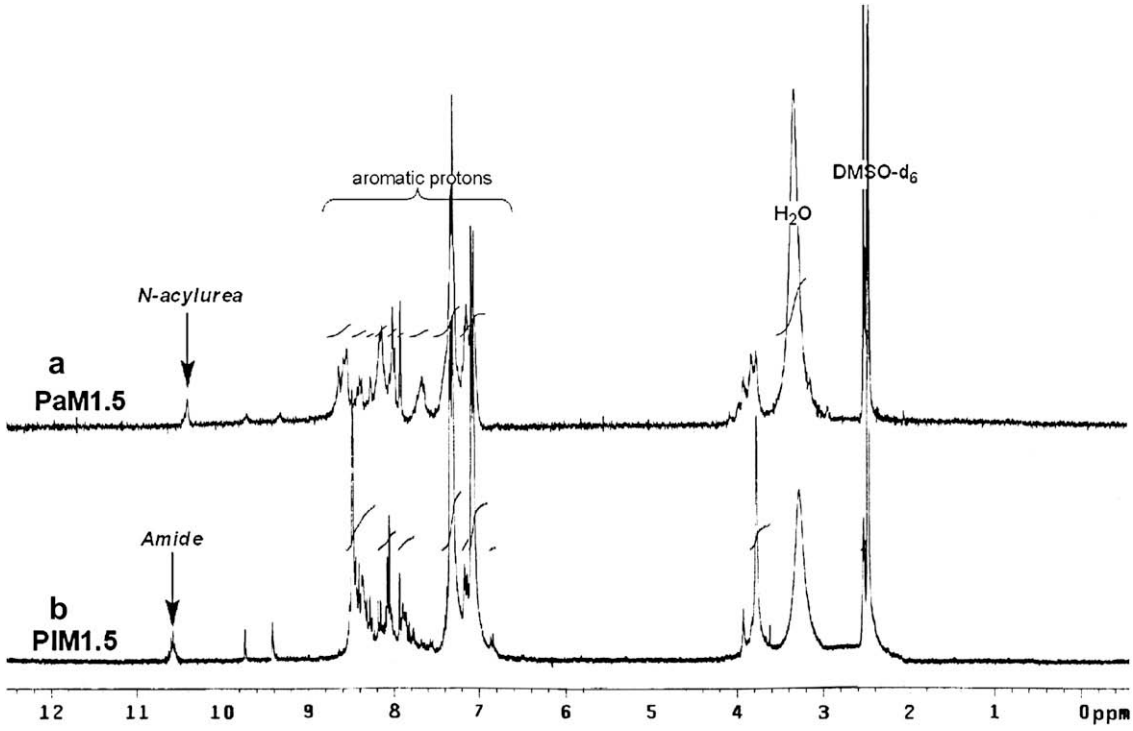

Fig. 3. ^{1}H NMR spectra of (a) PaM1.5 and (b) PIM1.5.

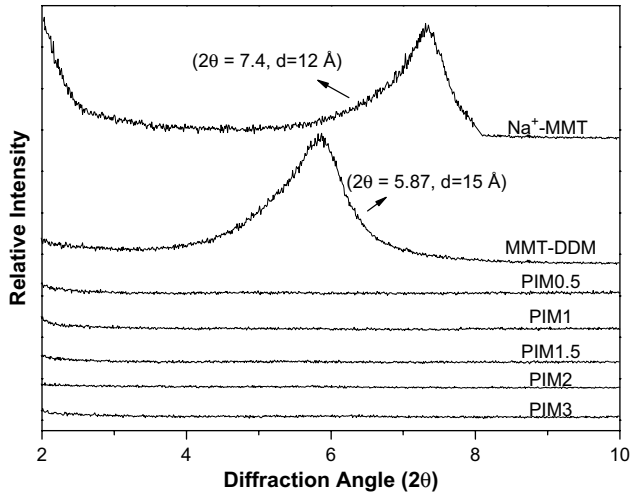

Fig. 4. XRD patterns for pristine MMT, MMT–DDM, and PIM samples with various inorganic contents.

polymer chains could easily diffuse into the in between layers of modified MMT. Apart from that, the solubility of PaDN and PaM samples in organic solvents such as DMF, DMAc, and DMSO is excellent. Because of the excellent organo-solubility, these samples could be easily processed into optical quality thin films by spin-coating. After SSRR, all of the NLO-active poly(amide-imide) and nanocomposites exhibited great solvent resistance.

Thermal properties of PIDN and PIM systems are summarized in Table 1.

The T_g of PIDN was observed as 191 °C. As the inorganic clay content increased, the T_g values of PIM samples first increased and then reached a maximum point at the inorganic ratio of 1.5%. Finally, the T_gs started to decline at the inorganic ratios of 2.0 and 3.0%. This indicates that the T_g value was enhanced by the incorporation of inorganic ratio at first, resulting from the barrier effect of the MMT layer structures, as well as the strong interaction between the organoclay and poly(amide-imide) [25]. In other words, the molecular motions of poly(amide-imide)s were inhibited by the silicate layers. However, further increase of clay loading (e.g. 2 and 3 wt%) was unable to enhance the T_gs of the PIM samples. This is possibly due to the aggregation of MMT as reported by Tyan and co-workers [34]. In addition, the thermal decomposition temperature (T_d) was measured using TGA under N_2 and air atmospheres, with regard to the weight loss of 5 wt%. The T_ds of PIDN and PIM samples are summarized in Table 1. The T_d values were observed at temperatures higher than 257 °C for all of the NLO-active nanocomposites.

3.3. TEM analysis of nanocomposites

The nanometer-scale dispersion of intercalated layered silicates in poly(amide-imide)s was further evidenced by TEM micrographs. The spatial distribution of inorganic silicates in the PIM nanocomposites is visualized in the TEM images. As shown in Fig. 5, the TEM images of PIM1 and PIM1.5 indicate the well-distribution of inorganic silicates in the polymer matrices, which is consistent with the XRD study mentioned earlier. Presumably, the spatially expanded interlayer space in MMT–DDM allows the accessibility of the polymer PaDNs for entering into the layered galleries and substantially reacting with the intercalating agent, DDM. Ultimately, the SSRR affords the PIM nanocomposites with the clay interlayer *d*-spacings to be further widened in the polymer matrices. The well-dispersed morphology of poly(amide-imide)–clay materials due to the presence of chemical bonding between the modified MMT and the polymer chains would result in better thermal properties [25]. Furthermore, the TEM image in Fig. 5c indicates that a mixed morphology is present for the PIM3 nanocomposite. Among the individual silicate layers, only part of them were intercalated in the poly(amide-imide) matrices, whereas the remnant displayed aggregated phenomenon. The aggregated phenomenon is possibly due to the number of poly(amide-imide) polymer chains being not large enough to resist the attraction between silicate interlayers [25]. Generally, the aggregation of MMT in PIM3 would lead to relatively poor thermal properties.

3.4. EO properties of poled/cured PIDN and PIM samples

In the investigation of optical properties, only the samples with better thermal stability (PIDN, PIM0.5, PIM1 and PIM1.5) were measured. For the sake of comparison, the PIM3 sample with relatively poor thermal stability was also investigated. Optical properties of these NLO poly(amide-imide)–clay nanocomposites are summarized in Table 1. The refractive indices of PIM system range from 1.70 to 1.72. The maximum absorption peak of UV–vis spectrum is closely related to the NLO-active dye in the polymer system. The λ_{max} values for the nanocomposites with DNDA were around 490 nm, which were similar to that of the pristine polymer. EO coefficients of PIM system that resulted from the in situ curing/poling process are in the range from 17 to 20 pm/V (measured at 830 nm). In fact, the EO signal would exhibit a reasonable error because of the wavelength dependence of laser pulse amplitude and the intrinsic fluctuations of the beam intensity [35]. Taking this into account, the results indicate that the EO coefficients were somewhat similar for these poled PIM samples. This is due to the presence of similar dye contents. The PIDN sample prepared via SSRR allows the dyes to orient easily towards the electric field direction prior to curing. As a result, larger EO coefficients were

Table 1
Characteristics of the PIDN and poly(amide-imide)–clay nanocomposites.

	Inorganic content (wt%)	Dye content[a](%)	T_d (°C) [b]		T_g (°C)[c]	Optical loss (dB/cm)		Refractive indices	r_{33} (pm/V)	Thermal dynamic stability (°C)[d]	Temporal stability [e]
			N_2	Air		830 nm	1310 nm				
PIDN	0	12.8	279	284	191	5.2	3.4	1.75	20	164	15%
PIM0.5	0.5	12.7	278	294	193	5.1	3.6	1.71	19	198	63%
PIM1	1.0	12.6	272	335	190	5.3	3.9	1.72	18	205	79%
PIM1.5	1.5	12.6	275	287	196	5.6	3.4	1.71	20	228	86%
PIM2	2.0	12.5	278	286	188	–[f]	–	–	–	–	–
PIM3	3.0	12.3	257	286	163	5.1	3.5	1.70	17	–	–

[a] The dye content was determined by UV–vis spectroscopic investigations.
[b] T_d was read at the temperature corresponding to 5% weight loss by TGA.
[c] Determined by DSC with a heating rate of 10 deg;C/min in nitrogen.
[d] Determined with a heating rate of 2 °C/min.
[e] Determined at 120 °C for 100 h.
[f] Not measured.

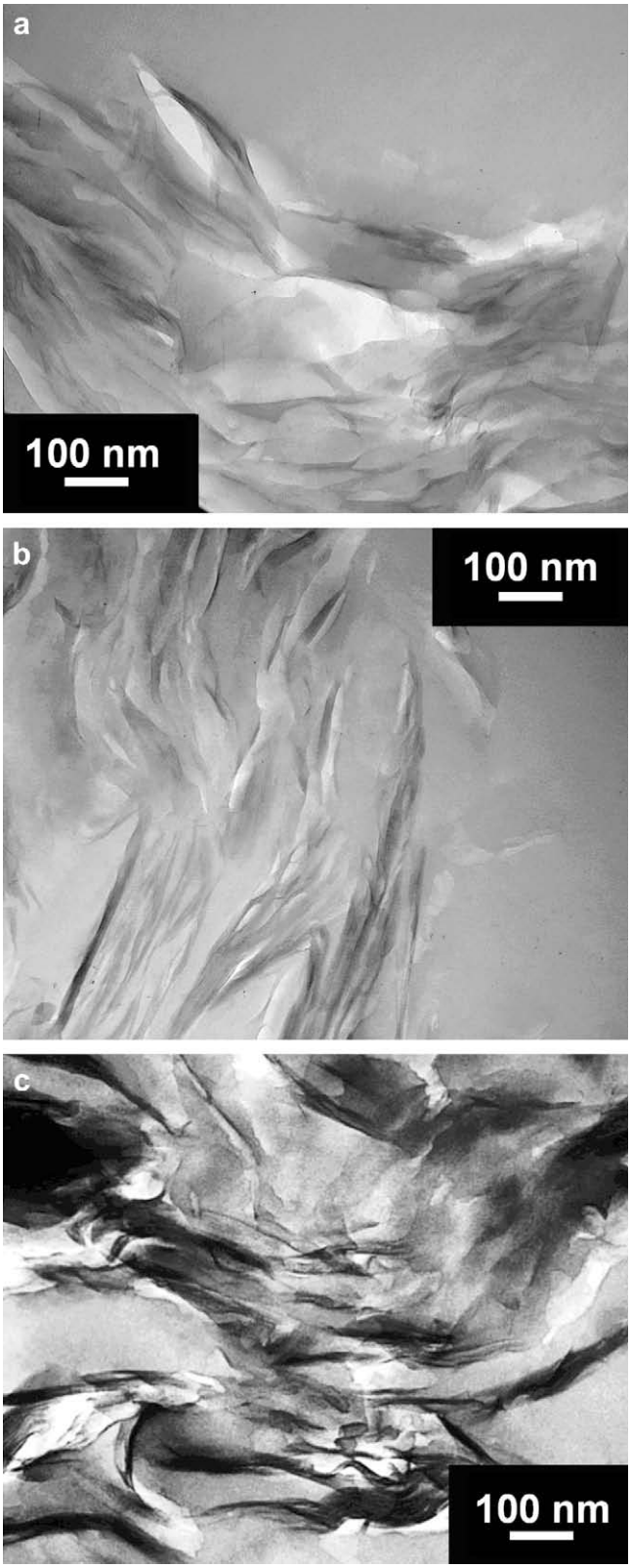

Fig. 5. TEM micrographs of (a) PIM1, (b) PIM1.5, and (c) PIM3.

obtained. PIDN, with a dye content of only 12.8 wt%, exhibited an r_{33} of 20 pm/V. Zhou et al. [36] and Qiu et al. [37] reported the preparation of stable NLO polyimides via traditional imidization between diamino-dye and dianhydride. The polyimides with four times as much of dyes (66 wt%) exhibited similar r_{33} coefficients close to 20 pm/V at 830 nm. Moreover, the existence of inorganic silicate layers did not interfere with the alignment of NLO dyes under the electric field, which is also attributed to the cause of similar EO coefficients. It is important to note that the thermal stability enhancement usually requires the presence of large quantities of the inorganic material in the organic–inorganic system via the sol–gel process. This would lead to a significant decrease of NLO density, i.e. optical nonlinearity [20]. In this work, by dispersing a small amount of organoclay into the NLO poly(amide-imide), the thermal properties can be increased noticeably without the disadvantage of the reduced NLO density.

In general, the EO coefficients of NLO polymers remain stable at low temperatures, but decay significantly at a specific temperature. This specific temperature is defined as the effective relaxation temperature [1]. This value provides information on maximum device operating temperatures that the film can endure, and allows quick evaluation of the temporal and thermal stability of the materials. PIDN, PIM0.5, PIM1 and PIM1.5 were chosen for further NLO stability study because of their relatively high T_gs. Temperature dependence of the dipole re-orientation dynamics of the poled/cured PIDN and PIM samples is shown in Fig. 6. The dynamic thermal stability of EO coefficient increased with increasing inorganic silicate content. The poled PIM1.5 sample exhibited a higher effective relaxation temperature (228 °C) as compared to PIM0.5 (198 °C) and PIM1 (205 °C) samples. This result is consistent with the T_gs of the polymeric nanocomposites mentioned earlier. Despite their similar T_gs, the PIM0.5 and PIM1 samples exhibited higher effective relaxation temperatures when compared to the pristine poly(amide-imide), PIDN. This demonstrates that the thermally stable layered MMT could effectively hinder the randomization of the aligned dyes in the polymer matrices. In addition, the temporal stability of EO coefficient for the poled/cured samples at 120 °C is shown in Fig. 7. Similarly, the PIM0.5 and PIM1 samples exhibited better temporal stability than the pristine PIDN sample. Moreover, a much better temporal stability was obtained for the PIM1.5 sample as compared to the PIDN, PIM0.5 and PIM1 samples. This indicates that the sample with an optimum amount of well-dispersed inorganic silicate layers could effectively enhance the temporal stability at elevated temperatures. In our previous research [25], a reactive organoclay was obtained using trifunctional amino compounds as an intercalating agent for MMT. One of the functional groups of the intercalating agents formed an ionic bond with the negatively charged silicates, whereas the remaining functional groups were available for further reaction with a poly(amic acid) end capped with anhydride groups. After poling

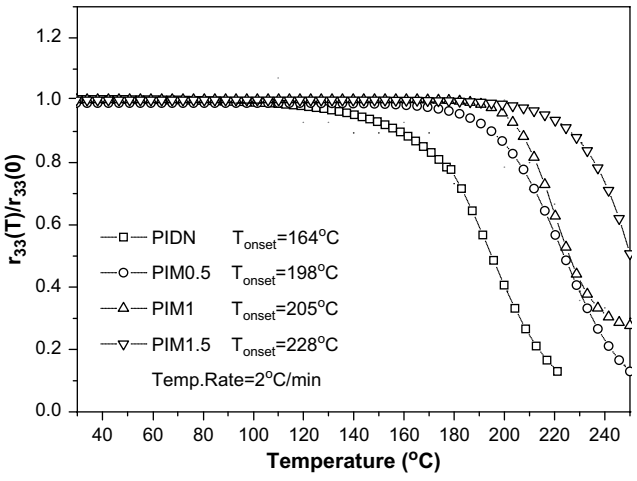

Fig. 6. Temperature dependence of the dipole re-orientational dynamics of the poled/cured PIDN and PIM samples.

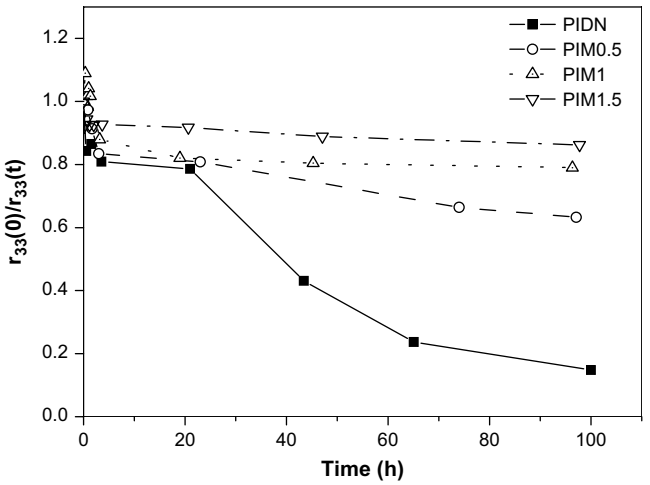

Fig. 7. Temporal behavior of the EO coefficient for the poled/cured PIDN and PIM samples at 120 °C.

and curing, the polyimide/MMT nanocomposites retained 75% of the original r_{33} value after being subjected to 100 °C thermal treatment for 100 h. In this work, a small portion of anhydride groups located throughout the poly(*N*-acylurea) chains would react with the amino groups of modified clay, resulting in greater interaction force to achieve excellent dispersion and compatibility between the layered silicates and the polymer. This would certainly lead to a much better temporal stability. PIM1.5 exhibited the best temporal stability while retaining 86% of the original r_{33} value after being subjected to 120 °C thermal treatment for 100 h. In addition, the inorganic ratio in PIM system was only 1.5%, which is much lower than that in the polyimide/MMT system reported earlier [25]. Yet the PIM1.5 sample possessed a much better temporal stability. Excellent thermal stability could be achieved with the addition of a small amount of well-dispersed MMT, while the electro-optical properties remained virtually unaffected.

3.5. Optical loss measurement

In the investigation of optical loss, the samples with better temporal stability (PIM0.5, PIM1, PIM1.5 and PIDN) and PIM3 were measured at 830 and 1310 nm under TE guide modes. As shown in Table 1, the optical losses of these NLO-active poly(amide-imide)–clay nanocomposite-based polymer waveguides are in the range 5.1–5.6 dB/cm and 3.4–3.9 dB/cm at 830 and 1310 nm, respectively. The number density of C–H, O–H and N–H bonds in the intrinsic structures plays a key role in deciding the optical loss of materials [38,39]. All of the NLO-active poly(amide-imide)s/inorganic clay nanocomposites exhibited the similar optical loss values. Optical loss was not increased with the addition of inorganic clay to the poly(amide-imide) matrices. This is attributed to the presence of well-dispersed nanoclay in the polymer. To further improve the optical loss properties of polymers, the loss can be limited by shifting C–H overtone vibrated absorption towards longer wavelengths by replacing hydrogen atoms with heavier atoms such as deuterium or halogens, essentially chlorine or fluorine [40,41].

4. Conclusion

NLO-active poly(amide-imide)–clay nanocomposites were prepared by a polymeric intermediate, poly(*N*-acylurea) consisting of organically modified MMT via SSRR. The anhydride groups are abundant along the polymer chains of poly(*N*-acylurea). These anhydride groups serve as multiple reactive sites that are available for reaction with the amino groups of modified clay, resulting in significantly enhanced interaction and well-dispersed layered silicates. Consequently, the ameliorated morphology of nanocomposites due to the rich chemical bonds between the intercalating agent-modified MMT and the polymer chains would bring about better thermal properties. Moreover, all of these poly(amide-imide)–clay nanocomposites show solvent resistance and waveguide properties after curing process. Not only could high dipole re-orientational dynamic temperatures be obtained, but excellent temporal stability of EO coefficient at 120 °C was also achieved.

Acknowledgement

Financial support from National Science Council of Taiwan and Chung-Shan Institute of Science and Technology is gratefully acknowledged. This work is also supported in part by the Ministry of Education, Taiwan under ATU plan.

References

[1] Prasad PN, Williams DJ. Introduction to nonlinear optical effects in molecules and polymers. New York: Wiley; 1991.
[2] Chang CC, Chen CP, Chou CC, Kuo WJ, Jeng RJ. Polymers for electro-optical modulation. Journal of Macromolecular Science, Part C: Polymer Reviews 2005;45:125–70.
[3] Singer KD, Sohn JE, Lalama SJ. Second harmonic generation in poled polymer films. Applied Physics Letters 1986;49(5):248–50.
[4] Sinyukov AM, Leahy MR, Hayden LM, Haller M, Luo J, Jen AKY, et al. Resonance enhanced THz generation in electro-optic polymers near the absorption maximum. Applied Physics Letters 2004;85(24):5827–9.
[5] Baehr JT, Hochberg M, Wang G, Lawson R, Liao Y, Sullivan PA, et al. Optical modulation and detection in slotted silicon waveguides. Optics Express 2005;13(14):5216–26.
[6] Chemla DS, Zyss J, editors. Nonlinear optical properties of organic molecules and crystals. New York: Academic Press; 1987.
[7] Tsutsumi N, Morishima M, Sakai W. Nonlinear optical (NLO) polymers. 3. NLO polyimide with dipole moments aligned transverse to the imide linkage. Macromolecules 1998;31(22):7764–9.
[8] Chen CP, Huang GS, Jeng RJ, Chou CC, Su WC, Chang HL. Low loss second-order non-linear optical crosslinked polymers based on a phosphorus-containing maleimide. Polymers for Advanced Technologies 2004;15:587–92.
[9] Jeng RJ, Jan LH, Lee RH. Thermally stable NLO materials based on organo-soluble polyimides and an alkoxysilane dye via sol–gel process. Journal of Macromolecular Science, Part A: Pure and Applied Chemistry 2001;A38(8):821–37.
[10] Jeng RJ, Chan LH, Lee RH, Hsiue GH, Chang HL. Polyimide/inorganic interpenetrating polymer networks for stable second-order nonlinear optics. Journal of Macromolecular Science, Part A: Pure and Applied Chemistry 2001;A38(12):1259–74.
[11] Kuo WJ, Hsiue GH, Jeng RJ. Synthesis and macroscopic second-order nonlinear optical properties of poly(ether imide)s containing a novel two-dimensional carbazole chromophore with nitro acceptors. Journal of Materials Chemistry 2002;12:868–78.
[12] Li Z, Li Z, Di C, Zhu Z, Li Q, Zeng Q, et al. Structural control of the side-chain chromophores to achieve highly efficient nonlinear optical polyurethanes. Macromolecules 2006;39(20):6951–61.
[13] Zeng Q, Li Z, Li Z, Ye C, Qin J, Tang BZ. Convenient attachment of highly polar azo chromophore moieties to disubstituted polyacetylene through polymer reactions by using "click" chemistry. Macromolecules 2007;40(16):5634–7.
[14] Zhu Z, Li Z, Tan Y, Li Z, Li Q, Zeng Q, et al. New hyperbranched polymers containing second-order nonlinear optical chromophores: synthesis and nonlinear optical characterization. Polymer 2006;47:7881–8.
[15] Li Q, Li Z, Ye C, Qin J. New indole-based chromophore-containing main-chain polyurethanes: architectural modification of isolation group, enhanced nonlinear optical property, and improved optical transparency. The Journal of Physical Chemistry B 2008;112(16):4928–33.
[16] Jeng RJ, Chen YM, Jain AK, Kumar J, Tripathy SK. Stable second-order nonlinear optical polyimide/inorganic composite. Chemistry of Materials 1992;4(6):1141–4.
[17] Jeng RJ, Hong WY, Chen CP, Hsiue GH. Organic/inorganic NLO materials based on reactive polyimides and a bulky alkoxysilane dye via sol/gel process. Polymers for Advanced Technologies 2003;14:66–75.
[18] Jeng RJ, Chang CC, Chen CP, Chen CT, Su WC. Thermally stable crosslinked NLO materials based on maleimides. Polymer 2003;44:143–55.
[19] Chang HL, Lin HL, Wang YC, Dai SA, Su WC, Jeng RJ. Thermally stable NLO poly(amide-imide)s via sequential self-repetitive reaction. Polymer 2007;48:2046–55.
[20] Lin HL, Chao TY, Shih YF, Dai SA, Su WC, Jeng RJ. Stable second-order nonlinear optical poly(amide-imide)/inorganic materials via simultaneous sequential

self-repetitive reaction and sol–gel process. Polymers for Advanced Technologies 2008;19:984–92.
[21] Dudkina MM, Tenkovtsev AV, Pospiech D, Jehnichen D, Haussler L, Leuteritz A. Nanocomposites of NLO chromophore-modified layered silicates and polypropylene. Journal of Polymer Science, Part B: Polymer Physics 2005;43:2493–502.
[22] Ogawa M, Ishikawa A. Controlled microstructures of amphiphilic cationic azobenzene–montmorillonite intercalation compounds. Journal of Materials Chemistry 1998;8(2):463–7.
[23] Coradin T, Nakatani K, Zyss J, Clenent R. Second harmonic generation of dye aggregates in bentonite clay. Journal of Materials Chemistry 1997;7(6):853–4.
[24] Neff GA, Helfrich MR, Clifton MC, Page CJ. Layer-by-layer growth of acentric multilayers of Zr and azobenzene bis(phosphonate): structure, composition, and second-order nonlinear optical properties. Chemistry of Materials 2000;12(8):2363–71.
[25] Chao TY, Chang HL, Su WC, Wu JY, Jeng RJ. Nonlinear optical polyimide/montmorillonite nanocomposites consisting of azobenzene dyes. Dyes and Pigments 2008;77:515–24.
[26] Chen YC, Juang TY, Dai SA, Wu TM, Lin JJ, Jeng RJ. Optical non-linearity from montmorillonite intercalated with a chromophore-containing dendritic structure: a self-assembly approach. Macromolecular Rapid Communications 2008;29(7):587–92.
[27] Tyan HL, Leu CM, Wei KH. Effect of reactivity of organics-modified montmorillonite on the thermal and mechanical properties of montmorillonite/polyimide nanocomposites. Chemistry of Materials 2001;13(1):222–6.
[28] Tyan HL, Liu YC, Wei KH. Enhancement of imidization of poly(amic acid) through forming poly(amic acid)/organoclay nanocomposites. Polymer 1999;40:4877–86.
[29] Wei KL, Wu CH, Huang WH, Lin JJ, Dai SA. *N*-Aryl acylureas as intermediates in sequential self-repetitive reactions to form poly(amide-imide)s. Macromolecules 2006;39(1):12–4.
[30] Huang Y, Paul DR. Experimental methods for tracking physical aging of thin glassy polymer films by gas permeation. Journal of Membrane Science 2004;244:167–78.
[31] Teng CC, Man HT. Simple reflection technique for measuring the electro-optic coefficient of poled polymers. Applied Physics Letters 1990;56(18):1734–6.
[32] Jeng RJ, Hsiue GH, Chen JI, Marturunkakul S, Li L, Jiang XL, et al. Low loss second-order nonlinear optical polymers based on all organic sol–gel materials. Journal of Applied Polymer Science 1995;55:209–14.
[33] Yang CP, Hsiao SH. Effects of various factors on the formation of high molecular weight polyamic acid. Journal of Applied Polymer Science 1985;30:2883–905.
[34] Tyan HL, Wei KH, Hsieh TE. Mechanical properties of clay–polyimide(BTDA-ODA) nanocomposites via ODA-modified organoclay. Journal of Polymer Science, Part B: Polymer Physics 2000;38:2873–81.
[35] Balducci A, De Sio A, Marinelli M, Milani E, Morgada ME, Pace E, et al. Extreme UV single crystal diamond photodetectors by chemical vapor deposition. Diamond and Related Materials 2005;14:1980–3.
[36] Zhou Y, Leng W, Liu X, Xu Q, Feng J, Liu J. Synthesis of nonlinear optical polyimides containing azodiamine derivative chromophores and their electro-optic and thermal properties. Journal of Polymer Science, Part A: Polymer Chemistry 2002;40:2478–86.
[37] Qiu F, Cao Y, Xu H, Jiang Y, Zhou Y, Liu J. Synthesis and properties of polymer containing azo-dye chromophores for nonlinear optical applications. Dyes and Pigments 2007;75:454–9.
[38] Shi W, Fang CS, Sui Y, Yin J, Pan QW, Gu QT, et al. Thermal stability and transmission losses of the poled polyimide side-chain thin films. Optics Communications 2000;183:299–306.
[39] Shi W, Fang CS, Sui Y, Yin J, Pan QW, Gu QT, et al. Poling optimization and optical loss measurement of the polyetherketone polymer films. Solid State Communications 2000;16:67–71.
[40] Wang C, Zhang C, Lee MS, Dalton LR, Zhang H, Steier WH. Urethane–urea copolymers containing siloxane linkages: enhanced temporal stability and low optical loss for second-order nonlinear optical applications. Macromolecules 2001;34:2359–63.
[41] Pitois C, Vukmirovic S, Hult A, Wiesmann D, Robertsson M. Low-loss passive optical waveguides based on photosensitive poly(pentafluorostyrene-*co*-glycidyl methacrylate). Macromolecules 1999;32:2903–9.